CI&CEQ
Chemical Industry & Chemical Engineering Quarterly

Available on line at
Association of the Chemical Engineers of Serbia *AChE*
www.ache.org.rs/CICEQ

*Chem. Ind. Chem. Eng. Q.* 22 (1) 65–73 (2016) CI&CEQ

ALEKSANDAR GOLUBOVIĆ[1]
IVANA VELJKOVIĆ[2]
MAJA ŠĆEPANOVIĆ[1]
MIRJANA GRUJIĆ-BROJČIN[1]
NATAŠA TOMIĆ[1]
DUŠAN MIJIN[3]
BILJANA BABIĆ[4]

[1]Institute of Physics, University of Belgrade, Belgrade, Serbia
[2]Institute for Multidisciplinary Research, University of Belgrade, Belgrade, Serbia
[3]Faculty of Technology and Metallurgy, University of Belgrade, Belgrade, Serbia
[4]Institute of Nuclear Sciences "Vinča", University of Belgrade, Belgrade, Serbia

SCIENTIFIC PAPER

UDC 54:66:544.526.5

DOI 10.2298/CICEQ150110020G

# INFLUENCE OF SOME SOL-GEL SYNTHESIS PARAMETERS OF MESOPOROUS $TIO_2$ ON PHOTOCATALYTIC DEGRADATION OF POLLUTANTS

**Article Highlights**

- Anatase nanopowders were synthesized by sol-gel method using tetrabutyl titanate as precursor
- XRPD data showed slight growth of crystallites in synthesized samples (from 24 to 35 nm)
- Raman scattering data confirmed the anatase as dominant $TiO_2$ phase
- The BET showed that specific surface area was greater at the lower temperature of calcination
- Photodegradations were comparable with Degussa P25 for C.I. Reactive Orange 16 and phenol

**Abstract**

*Titanium dioxide ($TiO_2$) nanopowders were produced by sol-gel technique from tetrabutyl titanate as a precursor by varying some parameters of the sol-gel synthesis, such as temperature (500 and 550 °C) and the duration of calcination (1.5, 2 and 2.5 h). X-ray powder diffraction (XRPD) results have shown that all synthesized nanopowders were dominantly in the anatase phase, with the presence of a small amount of rutile in samples calcined at 550 °C. According to the results obtained by the Williamson-Hall method, the anatase crystallite size was increased with the duration of the calcination (from 24 to 29 nm in samples calcined at lower temperature, and from 30 to 35 nm in samples calcined at higher temperature). The analysis of the shift and linewidth of the most intensive anatase $E_g$ Raman mode confirmed the XRPD results. The analysis of pore structure from nitrogen sorption experimental data described all samples as mesoporous, with mean pore diameters in the range of 5-8 nm. Nanopowder properties have been related to the photocatalytic activity, tested in degradation of the textile dye (C.I. Reactive Orange 16), carbofuran and phenol.*

*Keywords: nanostructures, anatase, X-ray diffraction, Raman scattering.*

Photocatalysis is a well-known process mostly employed to degrade or transform organic and inorganic compounds, and the kinetics depend on catalyst surface area, availability of active sites, pore sizes, number and nature of trapped sites, as well as on adsorption/desorption characteristics. $TiO_2$ is an important photocatalyst mainly because of its strong oxidizing power, non-toxicity and long-term photostability. Nanocrystalline $TiO_2$ is essentially a cheap and biocompatible wide band-gap semiconductor with an involving photogenerated holes and photocatalytic capabilities for organic pollutants [1-3]. Namely, many organic compounds can be decomposed in aqueous solution in the presence of $TiO_2$ powders or coatings illuminated with near ultraviolet (UV) or visible light. The structural, morphological, optical and photocatalytic properties of $TiO_2$ nanocrystals are strongly dependent on the synthesis process [4,5]. Among the various synthesis methods, the sol-gel method has recently attracted a lot of attention, since it is simple and cost-effective way of producing nanostructured anatase $TiO_2$ with tailored properties.

Correspondence: A. Golubović, Institute of Physics, University of Belgrade, Pregrevica 118, 11080 Belgrade, Serbia.
E-mail: golubovic@ipb.ac.rs
Paper received: 10 January, 2015
Paper revised: 7 April, 2015
Paper accepted: 30 June, 2015

Many factors influence photocatalytic reactivity of $TiO_2$ which is documented by numerous publications in the last decades [6-11]. Generally, anatase is considered a desirable phase for photocatalysis application as it shows higher activity then rutile [8,12--13]. However, a mixture of anatase and rutile with a sintered interface, like commercial $TiO_2$ (Degusa P25), is claimed to be more active then pure anatase [14-17]. In order to obtain the highest performance, the main challenge is the synthesis of preferably nanocrystalline anatase $TiO_2$ that enables a balance between major influencing parameters: crystal structure, surface hydroxylation and crystallinity.

The sol-gel process represents a flexible chemical route to synthesize various high-performance nanostructured ceramic materials with controlled internal morphology and chemistry. Materials with designed internal nanostructure (entirely interconnected open nanoporosity, hierarchical, fractal or nanocrystalline solid network) and various possible chemical compositions (from organic to inorganic) can be obtained in large range of shapes (finely divided nanopowders, nanoparticles, thin and thick films, fibers, granular beds and monolithic materials). The sol-gel process is a solution-based technique, where the material structure is created through chemical reactions in the liquid state, giving the high flexibility of the process for easy application.

The photocatalytic efficiency of $TiO_2$ powder heavily depends on its microstructure and physical properties, which are in turn determined by the preparation conditions. Among these, the presence of mesopores gives rise to a large surface area, which offers abundant interaction sites with external molecules [18]. The photocatalytic process involves the separation of the electron-hole charge pair, their transport and trapping to/at the surface, and, finally, their reaction with the desired molecules. These processes always compete with the charge pair recombination. The nanostructure significantly affects these elemental processes based on several reasons. Apart from a high surface-to-volume ratio, which must be beneficial for all chemical processes, the first factor is the quantum confinement and improved reduction/ /oxidation power. The second factor is the practical absence of band bending and the consequent easier access of both charged particles to the surface [19].

$TiO_2$ nanopowders are very efficient compounds for the photodegradation of many pollutants [20,21]. In our investigations, we made a focus on degradation of organic pollutants having different chemical structure. Namely, a textile dye (C.I. Reactive Orange 16) [22,23], an insecticide (carbofuran [2,24-26]) and a phenol [27,28]. The commercial $TiO_2$ (Degussa P25) was applied in a number of photodegradation processes of pollutants, and we wanted to synthesize $TiO_2$ nanopowders using various parameters of synthesis and to compare the photocatalytic properties of such prepared catalysts. The mechanism of the photodegradation process is not completely defined, as many parameters are involved. According to this, our manuscript is a contribution in understanding of such a complex process. To the best of our knowledge, this study is original and it was not found in the literature.

Several methods of characterization, such as XRPD, Brunauer-Emmett-Teller (BET) measurements, and Raman scattering were employed in this study to correlate structural and morphological properties of synthesized $TiO_2$ nanopowders and their photocatalytic activity under UV light irradiation.

## EXPERIMENTAL

### Synthesis

The $TiO_2$ nanocrystals were prepared by a sol-gel method. All of the reagents were of analytical grade and were obtained from commercial sources and used without further purification. Tetrabutyl titanate (99%, Acros Organics, Belgium) was used as the precursor of titania, hydrochloride acid (36.2%, Zorka, Serbia) as the catalyst, ethanol (96%, denatured, Carlo Erba, Italy) as the solvent, and distilled water for hydrolysis. pH of the solution was 7. The reagent molar ratio was $Ti(OBu)_4$:HCl:EtOH:$H_2O$ = = 1:0.3:15:4 according to [29], which enabled obtaining a stable gel. The process of gelation was carried out at 4 °C, where appropriate amounts of $Ti(OBu)_4$, HCl and EtOH were stirred one hour by magnetic stirrer. After that, an appropriate amount of distilled water was added in the mixture due to hydrolysis and formation of the gel. This gel was “aged” (the process of polycondensation) for two hours, the wet gels were dried at 80 °C, and then calcinated at 500 and 550 °C for 1.5, 2 and 2.5 h, to obtain $TiO_2$ nanocrystals. The heating and the cooling rates were 135 °C/h. According to the calcination conditions (various temperature of calcinations and duration of the calcinations), synthesized samples were labeled as: $T_{500/1.5}$, $T_{500/2}$, $T_{500/2.5}$, $T_{550/1.5}$, $T_{550/2}$ and $T_{550/2.5}$.

### Characterization methods

Generally, instrumental broadening is negligible in the case of low crystallinity samples. Broadening of the peaks because of low crystallinity is dominant. These are fundamentals of X-ray powder analysis.

Structural analysis of prepared samples was done by XRPD on an Ital Structures APD2000 diffractometer, using CuKα radiation ($\lambda$ = 1.5406 Å), angular range: 20°< 2$\theta$ < 90°. Data were collected at every 0.01° in the 20-90° 2$\theta$ using a counting time of 80 s/step. MDI Jade 5.0 software was used for calculation of the structural and microstructural parameters. The Williamson-Hall method [30] was applied for the determination of average microstrain and the mean crystallite sizes, <*D*>, of the prepared samples. The obtained values were compared to the mean crystallite sizes calculated by the Scherrer formula [31]. The Scheerer formula is an estimate of crystallite size calculated from FWHM of all diffractions collected during measurement.

Raman scattering measurements was performed in the backscattering geometry at room temperature in air, using Jobin-Yvon T64000 triple spectrometer, equipped with a confocal microscope and a nitrogen-cooled coupled device detector. The spectra, excited by 514.5 nm line of $Ar^+/Kr^+$ laser with output power less than 5 mW to avoid local heating due to laser irradiation, was recorded with high spectral resolution of about 0.7 $cm^{-1}$.

The porous structure of anatase samples is evaluated from adsorption/desorption isotherms of $N_2$ at -196 °C, using the gravimetric McBain method. The main parameters of the porosity, such as specific surface area and pore volume, have been estimated by BET method from $\alpha_s$-plot [32]. The pore size distribution was estimated from hysteresis sorption data by the Barret-Joyner-Halenda (BJH) method [33].

### Measurements of photocatalytic activity

UV irradiation of a suspension (an appropriate amounts of pollutant and $TiO_2$ powder as the catalyst) was performed in an open flask (100 ml volume) with an Osram Ultra-Vitalux® 300 W (UV-A) lamp placed 50 cm from the surface of the solution. The light intensity was 40 mW $cm^{-2}$, and it was measured on the Amprobe Solar-100, Solar Power meter, Beha-Amprobe, GmbH. The textile dye, C.I. Reactive Orange 16, was obtained from the company Bezema, Switzerland, as a gift (commercial name Bezaktiv Orange V-3R) and used without futher purification. Carbofuran (99.2 %) was obtained from FMC, USA. Phenol, p.a. grade, was purchased from Fluka. The photodegradation of organic pollutants was studied by preparing a solution containing known concentration of organic and appropriate amount of $TiO_2$. In a typical experiment, 25 ml of a solution was used, the quantity of $TiO_2$ was 50 mg, whereas the pollutants solution molarities were $8.1\times10^{-5}$ M (C.I. Reactive Orange 16), $6.86\times10^{-4}$ M (carbofuran), $4\times10^{-4}$M (phenol), respectively. Upon preparation of the solution, agitation was applied in dark by continuous stirring (magnetic stirrer) at 400 rpm to keep the suspension homogenous for 90 min. Then, the lamp was switched on and the suspension sampled after appropriate times of irradiation. The concentration of pollutants was determined after centrifugation of a sample on Mini Spin Eppendorf at 12000 rpm by a UV-Vis spectrophotometer (Shimadzu 1700) at appropriate wavelength.

## RESULTS AND DISCUSSION

### XRPD measurements

The XRPD measurement confirmed that sol-gel synthesis resulted with preparation of anatase modification of $TiO_2$, which is clearly indicated with the main anatase reflection at 2$\theta \approx 25°$ (JCPDS card no. 21-1272). The samples calcinated at 500 °C were found to be phase-pure anatase (Figure 1), with crystallite sizes growing with increasing calcination time (Table 1), while the samples calcinated at 550 °C have small amount of rutile impurities, which are confirmed by small peaks at 2$\theta \approx 27°$ in Figure 1 (JCPDS, card no. 21-1276). The presence of rutile in calcined anatase samples can be caused both by pH value and the temperature of the calcination [34]. In our case, the small amount of rutile in samples calcined at 550 °C is caused by the temperature of the calcination as pH value is the same (pH 7).

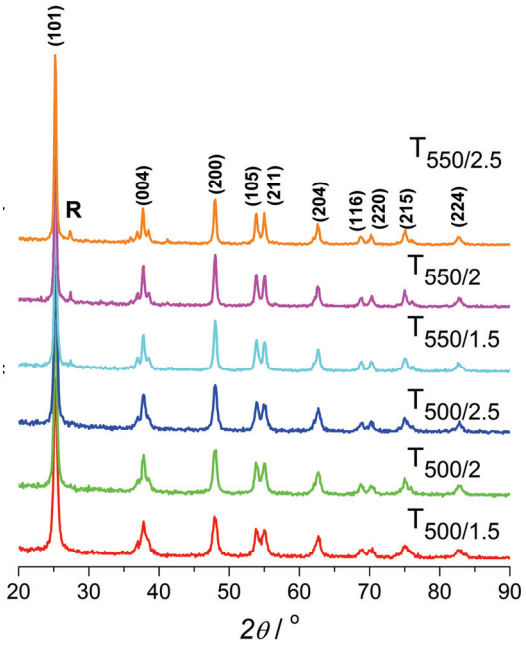


*Figure 1. The XRPD patterns of $TiO_2$ samples, where rutile diffraction is denoted by "R".*

*Table 1. The unit cell parameters and unit cell volume, together with average crystallite size, <D>, of anatase and microstrain obtained by Scherrer and Williamson-Hall methods*

| Sample | Calcination conditions | | Unit cell parameters | Scherrer method | Williamson-Hall method | |
|---|---|---|---|---|---|---|
| | Temperature, °C | Time, h | *a* and *c* in Å, *V* in Å$^3$ | <*D*> / nm | <*D*> / nm | Microstrain, % |
| $T_{500/1.5}$ | 500 | 1.5 | *a* = 3.784(3)<br>*c* = 9.53(0)<br>*V* = 136.4(8) | 15 | 24 | 0.301 |
| $T_{500/2}$ | 500 | 2.0 | *a* = 3.789(9)<br>*c* = 9.52(1)<br>*V* = 136.7(5) | 18 | 28 | 0.231 |
| $T_{500/2.5}$ | 500 | 2.5 | *a* = 3.789(2)<br>*c* = 9.50(3)<br>*V* = 136.4(5) | 19 | 29 | 0.247 |
| $T_{550/1.5}$ | 550 | 1.5 | *a* = 3.789(1)<br>*c* = 9.51(5)<br>*V* = 136.6(1) | 24 | 30 | 0.108 |
| $T_{550/2}$ | 550 | 2.0 | *a* = 3.788(7)<br>*c* = 9.51(4)<br>*V* = 136.5(7) | 28 | 33 | 0.077 |
| $T_{550/2.5}$ | 550 | 2.5 | *a* = 3.789(1)<br>*c* = 9.53(4)<br>*V* = 136.8(9) | 30 | 35 | 0.085 |

According to the Scherrer formula, the crystallite size for samples calcinated at lower temperature has been estimated in the range from 15 to 19 nm, while the samples calcinated at higher temperature have higher crystallinity, with crystallite size in the range from 24 to 30 nm, while for these estimated by Williamson-Hall method were in the range from 24 to 29 nm for lower temperature and from 30 to 35 nm for higher temperature. The analysis of XRPD data by the Williamson-Hall method has shown higher microstrain value in the samples calcinated at 500 °C compared to the samples calcinated at 550 °C. In all futher discussion, values of crystalline size evaluated by the Williamson-Hall method were used.

## Raman scattering measurements

The Raman spectra of all synthesized nanopowders are dominated by anatase Raman modes [35,36]: $E_{g(1)}$ (~143 cm$^{-1}$), $E_{g(2)}$ (~199 cm$^{-1}$), $B_{1g}$ (~399 cm$^{-1}$), $A_{1g}$+$B_{1g}$ (~518 cm$^{-1}$), and $E_{g(3)}$ (~639 cm$^{-1}$), as can be seen from the spectrum of two chosen samples shown in Figure 2. The most intensive Raman $E_{g(1)}$ mode is positioned between 142.8 and 143.5 cm$^{-1}$, with linewidths from 9 to 11.5 cm$^{-1}$. The dependence of Raman shift on linewidth of this mode is shown in Figure 3. The $E_{g(1)}$ Raman modes in the samples $T_{500/1.5}$, $T_{500/2}$ and $T_{500/2.5}$, calcined at lower temperature (500 °C), are more shifted and more broadened then the mode in samples calcined at higher temperature (550 °C). Having in mind the relatively large crystallite size in all samples registered

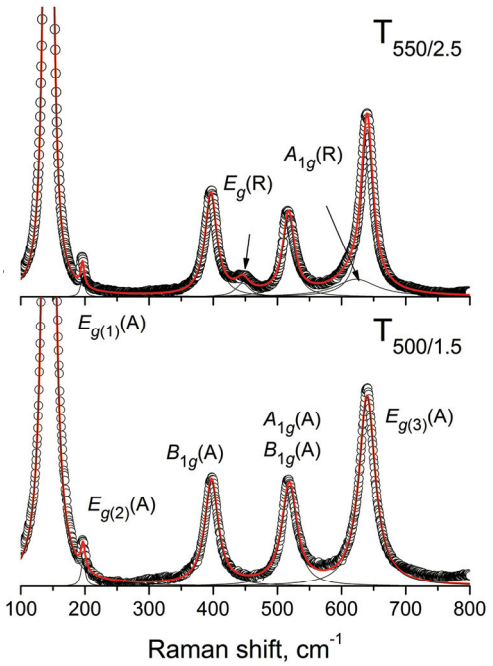


*Figure 2. The Raman spectra of samples $T_{500/1.5}$ and $T_{550/2.5}$. The experimental spectra (circles) are fitted by the sum of Lorentzians (thin lines). Anatas modes are denoted by "A" and rutile by "R".*

by XRPD (24-35 nm), slight shift and broadening relative to bulk anatase [33] may rather be ascribed to defects and disorder in anatase crystal structure, than to the phonon confinement effects. The smaller linewidth and the Raman shift of Degussa P25 compared

to the series of obtained samples can be explained as the least deffective and disordered anatase structure.

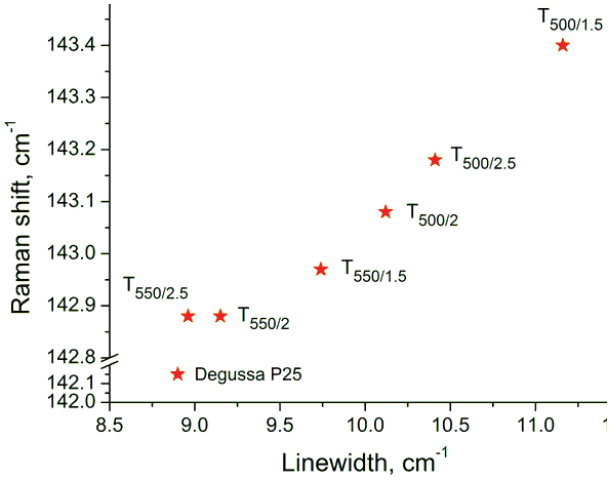


*Figure 3. The experimental dependence of Raman shift on linewidth for the most intensive $E_{g(1)}$ mode of synthesized anatase samples and Degussa P25.*

Some additional Raman features, detected in the sample $T_{550/2.5}$ shown in Figure 2, can be ascribed to the rutile modes [37] $E_g$ (~445 $cm^{-1}$) and $A_{1g}$ (~609 $cm^{-1}$). The Raman modes related to the brookite phase [38] in the synthesized samples were not detected.

## Porosity

To investigate the effects of synthesis conditions parameters on the adsorption abilities and pore structure of $TiO_2$ samples, the nitrogen sorption isotherms measurements have been carried out. The specific surface area, pore volume and mean pore diameter calculated from both BET and BJH are listed in Table 2. The samples calcined at 500 °C (samples $T_{500/1.5}$, $T_{500/2}$ and $T_{500/2.5}$) are obviously more porous than those calcined at 550 °C (samples $T_{550/1.5}$ and $T_{550/2.5}$). Note that the parameters of porosity, determined from the $\alpha_s$-plots [16,39], suggest that the samples are fully mesoporous ($S_{meso}$ = $S_{BET}$), whereas in the sample $T_{550/2}$ the porosity was very small (the pore concentration is within experimental error). The mean pore diameters obtained by BET and BJH method are in good agreement. The pore size distribution for synthesized anatase samples and Degussa P25, obtained by BJH method, are shown in Figure 4. It could be seen that in the rows $T_{500/1.5}$, $T_{500/2}$, $T_{500/2.5}$ and $T_{550/1.5}$, $T_{550/2}$, $T_{550/2.5}$ value of specific surface area had the highest value for the first member, lowest for the second and close to the first for the third member. The explanation for this tendency lies in the fact that the pores tranformed during the time of calcination. The tendency of microstrain in Table 1 was in accordance with the tendency of a pore evolution. Also, the pores in the samples calcined at 500 °C (mean pore diameter around 5-6 nm) are smaller than those in the samples calcined at higher temperature (7-8 nm), as can be seen in Table 2. From Figure 4 can be also

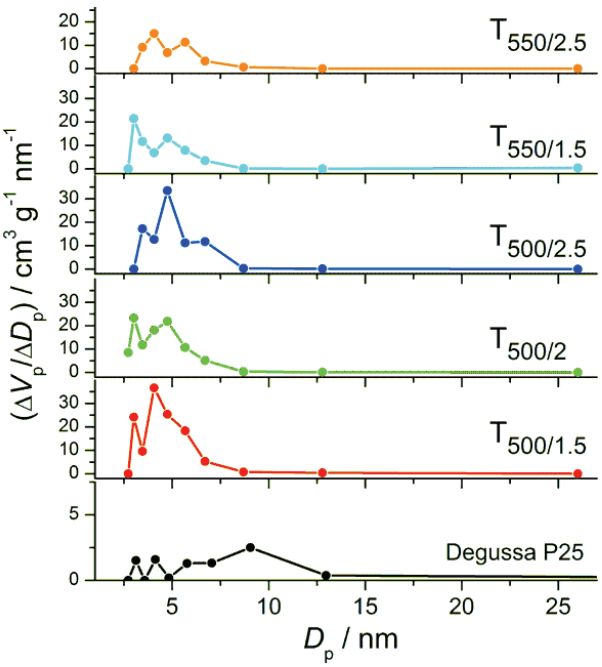


*Figure 4. The pore size distribution for synthesized anatase sample and Degussa P25 obtained by BJH method.*

*Table 2. The porous properties of synthesized anatase samples, as well as Degussa P25: specific surface areas ($S_{BET}$, $S_{BJH}$), pore volumes ($V_p$, $V_t$), and mean pore diameters ($\bar{D}_{BET}$ , $\bar{D}_{BJH}$ ) obtained by BET and BJH methods, respectively*

| Sample | $S_{BET}$ = $S_{meso}$, in $m^2$/g | $V_p$ / $cm^3$ $g^{-1}$ | $\bar{D}_{BET}$ / nm | $S_{BJH}$ / $m^2$ $g^{-1}$ | $V_t$ / $cm^3$ $g^{-1}$ | $\bar{D}_{BJH}$ / nm |
|---|---|---|---|---|---|---|
| $T_{500/1.5}$ | 52 | 0.1063 | 5.3 | 52.0 | 0.1025 | 5.1 |
| $T_{500/2}$ | 33 | 0.0757 | 5.9 | 34.2 | 0.0777 | 5.9 |
| $T_{500/2.5}$ | 45 | 0.0922 | 5.3 | 45.9 | 0.0903 | 5.1 |
| $T_{550/1.5}$ | 18 | 0.0580 | 8.3 | 18.5 | 0.0599 | 8.3 |
| $T_{550/2}$ | 2 | - | - | - | - | - |
| $T_{550/2.5}$ | 17 | 0.0454 | 6.9 | 18.3 | 0.0504 | 7.1 |
| Degussa P25 | 13 | 0.0244 | 7.5 | 11.6 | 0.0214 | 7.4 |

seen that the pore distribution of Degussa 25 was almost uniform (except for the largest value of about 9 nm) and that could be the crucial fact why Degussa 25 was the powerful tool for the photocatalytic degradation.

### Photocatalytic activity

The photocatalytic activity of synthesized catalyst was studied using three representatives of organic pollutants: C.I. Reactive Orange 16 (textile dye), carbofuran (pesticide) and phenol. The samples were (after mixting with pollutants, sorption and UV irradiation) withdrawn and analyzed on a UV-Vis spectrophotometer at 492.5 nm for C.I. Reactive Orange 16, 277 nm for carbofuran and 270 nm for phenol. The time after the agitation 90 min in dark is denoted as 0, and these concentrations are denoted as $c_0$. The reactions were performed using Degussa P25 $TiO_2$ for comparison. The results are shown in Figure 5.

In Figure 5a, the effectiveness of synthesized $TiO_2$ catalysts in photodegradation reaction of (C.I. Reactive Orange 16) is presented. In comparison to Degussa P25, the catalyst $T_{500/1.5}$ showed almost the same photodegradation effectiveness (99 and 98% after 90 min of UV irradiation, respectively), while the others samples, except $T_{550/1.5}$, showed similarly good photodegradation effectiveness. The photodegradation efficiency can be determined as:

$$\text{Efficiency} = 100\frac{c_0 - c}{c_0}$$

where $c_0$ is the initial concentration of pollutant solution and $c$ is the concentration after irradiation with UV light. The efficiencies of the studied $TiO_2$ catalysts as well as the observed pseudo first reaction rate constants were presented in Table 3. The main difference between Degussa P25 and synthesized catalysts is the reaction rate as a result of pore distribution uniformity.

In case of carbofuran, Degussa P25 showed higher photodegradation efficiency than all synthesized samples (98% of carbofuran was photodegraded after 90 min). After 150 min of UV irradiation, the highest photodegradation efficiency was obtained by samples $T_{500/1.5}$ (75%), whereas the lowest efficiency were observed for the samples $T_{550/1.5}$ and $T_{550/2.5}$ (both 49%). The obtained results are in accordance with the pore distribution influence on the reaction rate. Photocatalitic degradation of carbofuran using synthesized of $TiO_2$ series and Degussa P25 as catalysts are presented in Figure 5b. Here, one can observe that the photocatalytic reaction rate is highest when Degussa P25 is used, while the differences between synthesized catalysts are much less pronounced. As given above, the observed reaction rate might be the result of the mean pore diameter range, and the combination of specific surface area and mean pore diameter.

Phenol [40] was also subjected to photodegradation using synthesized catalysts and the results are shown in Figure 5c. It appears that $TiO_2$ (both synthesized and Degussa P25) is able to remove phenol too, but it requires more time, since the concentrations continuously decrease. After 150 min of

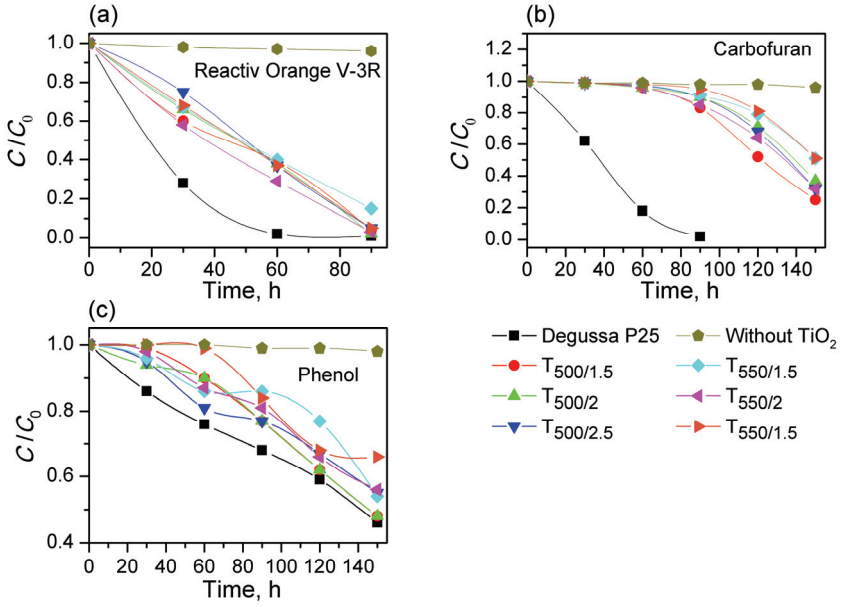


*Figure 5. The kinetics of degradation of: a) C.I. Reactive Orange 16, b) carbofuran and c) phenol, under UV irradiation monitored in the presence of synthesized $TiO_2$ samples and Degussa P25.*

*Table 3. The efficiency, %, of the studied $TiO_2$ catalysts as well as the observed pseudo-first reaction rate constants*

| Time, min | Catalyst | | | | | | |
|---|---|---|---|---|---|---|---|
| | P-25 | $T_{500/1.5}$ | $T_{500/2}$ | $T_{500/2.5}$ | $T_{550/1.5}$ | $T_{550/2}$ | $T_{550/2.5}$ |
| | | | | RO16 | | | |
| 0 | 0 | 0 | 0 | 0 | 0 | 0 | 0 |
| 30 | 72 | 40 | 34 | 25 | 33 | 42 | 32 |
| 60 | 98 | 61 | 62 | 63 | 60 | 71 | 63 |
| 90 | 99 | 96 | 98 | 95 | 85 | 97 | 95 |
| $k$ / min$^{-1}$ | 0.0546 | 0.0287 | 0.0335 | 0.0271 | 0.0189 | 0.0322 | 0.0271 |
| | | | | Carbofuran | | | |
| 0 | 0 | 0 | 0 | 0 | 0 | 0 | 0 |
| 30 | 38 | 1 | 1 | 1 | 1 | 1 | 1 |
| 60 | 82 | 4 | 4 | 3 | 2 | 4 | 2 |
| 90 | 98 | 17 | 10 | 10 | 9 | 15 | 5 |
| 120 | | 48 | 29 | 32 | 21 | 36 | 19 |
| 150 | | 75 | 63 | 68 | 49 | 68 | 49 |
| $k$ / min$^{-1}$ | 0.0372 | 0.0062 | 0.0041 | 0.0027 | 0.0028 | 0.0049 | 0.0027 |
| | | | | Phenol | | | |
| 0 | 0 | 0 | 0 | 0 | 0 | 0 | 0 |
| 30 | 14 | 1 | 6 | 5 | 4 | 2 | 0 |
| 60 | 24 | 10 | 10 | 19 | 14 | 13 | 1 |
| 90 | 32 | 23 | 23 | 23 | 14 | 19 | 16 |
| 120 | 41 | 38 | 38 | 33 | 23 | 34 | 32 |
| 150 | 54 | 52 | 52 | 45 | 46 | 44 | 34 |
| $k$ / min$^{-1}$ | 0.0048 | 0.004 | 0.004 | 0.0035 | 0.003 | 0.0033 | 0.0025 |

UV irradiation, Degussa P25 degraded 54%, almost the same value as for $T_{500/1.5}$ and $T_{500/2}$ (52%). Other samples ($T_{500/2.5}$, $T_{550/1.5}$ and $T_{550/2}$) degraded about 45% and $T_{550/2.5}$ showed the worst result (34%). Obtained photodegradation result for Degussa P25 is in accordance with results from de la Cruz Romero *et al*. [3] where phenol was not 100% photodegraded even with the UV irradiation of 10 h (only 60% under similar experimental conditions).

One would expect that the smaller molecule, phenol, can easily access the internal surface of Degussa sample giving higher degradation rate in comparison to other two organic pollutants. Namely, if only size of the molecule is important, than the reaction rate order would be: phenol > carbofuran > > RO16. On the contrary, the rate order is inverse, RO16 being most reactive. The main reason for such reaction rate is due to the different mechanisms of degradation and different part of molecules involved. If only one molecule is concerned, then the influence of the catalyst is more complex. Not only the mean pore diameter is important, but also the combination of specific surface area and mean pore diameter, giving Degussa an advantage when voluminous molecules are concerned.

## CONCLUSIONS

The structural and morphological properties of $TiO_2$ powders were intentionally varied by the temperature and duration of the calcination. The analysis of XRPD data showed that rising of temperature and extending the duration of the calcination caused slight growth of crystallites in synthesized samples (from 24 to 35 nm), which was confirmed by Raman scattering. It was also noticed that the most intensive Raman $E_g$ mode in the samples calcined at higher temperature (550 °C) is less broadened and blueshifted than in the samples calcined at 500 °C, pointing to less deffective and disordered anatase structure. The BET analysis showed that the greatest specific surface area was in the sample calcined for 1.5 h at 550 °C ($T_{550/1.5}$). The samples calcined at 500 °C displayed higher photocatalytic activity in the degradation in comparison with the samples calcined at 550 °C. The results of photodegradation of C.I. Reactive Orange 16 for the sample calcined 2 h at 500 °C (sample $T_{500/2}$) was comparable with Degussa P25. The samples calcined for 1.5 and 2 h at the same temperature (samples $T_{500/1.5}$ and $T_{500/2}$) showed comparable efficiency with Degussa P25 in photodegradation of phenol, while in

photodegradation of carbofuran Degussa P25 showed superior photocatalytic properties.

## Acknowledgement

This work was financially supported by the Serbian Ministry of Education, Science and Technological Development, Projects No. III45018 and ON171032, as well as SASA project F-134.

## REFERENCES

[1] R. Pourata, A. R. Khataee, S. Aber, N. Daneshvar, Desalination **249** (2009) 301-307

[2] M. Mahalakshmi, B. Arabindoo, M. Palanichamy, V. Murugesan, J. Hazard. Mater. **143** (2007) 240-245

[3] D. de la Cruz Romero, G. Torres Torres, J. C. Arévalo, R. Gomez, A. Aguilar-Elguezabal, *J. Sol-Gel Sci. Technol.* **56** (2010) 219-226

[4] Y. Wang, A. Zhou, Z. Yang, Mater. Lett. **62** (2008) 1930--1932

[5] Hari-Bala,Y. Guo, X. Zhao, J Zhao, W. Fu, X. Ding, Y. Jiang, K. Yu, X. Lv, Z. Wang, Mater. Lett. **60** (2006) 494--498

[6] W. Dong, Y. Sun, C. W. Lee, W. Hua, X. Lu, Y. Shi, S. Zhang, J. Chen, D. Zhao, J. Am. Chem. Soc. **129** (2007) 13894-13904

[7] E. Stathatos, D. Papoulis, C. A. Aggelopoulos, D. Panagiotaras, A. Nikolopoulou, J. Hazard. Mater. **211-212** (2012) 68-76

[8] T. Ohno, K. Sarukawa, M. Matsumura, New J. Chem. **26** (2002) 1167-1170

[9] M. Inagaki, R. Nonaka, B. Tryba, A. W. Morawski, Chemosphere **64** (2006) 437-445

[10] A. Sclafani, L. Palmisano, M. Schiavello, J. Phys. Chem. **94** (1990) 829-832

[11] N. Serpone, D. Lawless, R. Khairutdinov, E. Pelizzetti, J. Phys. Chem. **99** (1995) 16655-16661

[12] T. Ohno, K. Sarukawa, M. Matsumura, J. Phys. Chem., B **105** (2001) 2417-2420

[13] K. Tanaka, M. F. V. Capule, T. Hisanaga Chem. Phys. Lett. **187** (1991) 73-76

[14] D.C. Hurum, K.A. Gray, T. Rajh, M.C. Thurnauer, J. Phys. Chem., B **109** (2004) 977-980

[15] J. Zhang, Q. Xu, Z. Feng, M. Li, C. Li, Angew. Chem. Int. Edit. **47** (2008) 1766-1769

[16] T. Kawahara, Y. Konishi, H. Tada, N. Tohge, J. Nishii, S. Ito, Angew. Chem. Int. Edit. **41** (2002) 2811-2813

[17] A. Zachariah, K. V. Baiju, S. Shukla, K. S. Deepa, J. James, K.G.K. Warrier, J. Phys. Chem., C **112** (2008) 11345-11356

[18] W. Li, X. Guo, Y. Zhu, Y. Hui, K. Kanamori, K. Nakanishi, J. Sol-Gel Sci. Technol. **67** (2013) 639-645

[19] M. Fernández-García, A. Martínez-Arias, J. C. Hanson, J. A. Rodriguez, Chem. Rev. **104** (2004) 4063-4104

[20] S. Ahmed, M.G. Rasul, W.N. Martens, R. Brown, M.A. Hashib, Desalination **261** (2010) 3-18

[21] S. Ahmed, M.G. Rasul, W.N. Martens, R. Brown, M.A. Hashib, Water Air Soil Pollut. **215** (2011) 3-29

[22] C.-Y. Chen, Water Air Soil Pollut. **202** (2009) 335-342

[23] D. Mijin, M. Radulović, D. Zlatić, P. Jovančić, Chem. Ind. Chem. Eng. Q. **13** (2007) 179-185

[24] B. Lopez-Alvarez, R.A. Torres-Palma, G. Peñuela, J. Hazard. Mater. **191** (2011) 196-203

[25] J. Fenoll, P. Hellín, P. Flores, C. M. Martínez, S. Navarro, J. Photochem. Photobiol., A **251** (2013) 33-40

[26] F. Javier Benitez, J.L. Acero, F.J. Real, J. Hazard. Mater. **89** (2002) 51-65

[27] M. Jesus, S. Benito, O. Aaron O, A.H. de Lasa, Chem. Eng. Sci. **78** (2012) 186-203

[28] K. Majeda, W. Lijun, A.H. Al-Muhtaseb, A.B. Albadarin, G.M. Walker, Chem. Eng. J. **213** (2012) 125-134

[29] Y.L. Du, Y. Deng, M.S. Zhang, J. Phys. Chem. Solids **67** (2006) 2405-2408

[30] G.K. Williamson, W.H. Hall, Acta Metall. **1** (1953) 22-31

[31] H.P. Klug, L.E. Alexander, X-Ray Diffraction Procedures: For Polycrystalline and Amorphous Materials, 2nd ed., Wiley-VCH, New York, 1974, p. 687

[32] K. Kaneko, C. Ishii, H. Kanoh, Y. Hanzawa, N. Setoyama, T. Suzuki, Adv. Colloid Interfac. Sci. **76-77** (1998) 295--320

[33] E.P. Barrett, L.G. Joyner, P.P. Halenda, J. Am. Chem. Soc. **73** (1951) 373-381

[34] W. Zhang, S. Chen, S. Yu, Y. Yin, J. Cryst. Growth **308** (2007) 122-129

[35] T. Ohsaka, F. Izumi, Y. Fujiki, J. Raman Spectrosc. **7** (1978) 321-324

[36] M.J. Šćepanović, M. Grujić-Brojčin, Z. Dohčević-Mitrović, Z.V. Popović, Appl. Phys., A **86** (2007) 365-371

[37] X. Wang, J. Shen, Q. Pan, J. Raman Spectrosc. **42** (2011) 1578-1582

[38] Y.-H. Zhang, C. K. Chan, J. F. Porter, W. Guo, J. Mater. Res. **13** (1998) 2602-2609

[39] A. Golubović, B. Abramović, M. Šćepanović, M. Grujić--Brojčin, S. Armaković, I. Veljković, B. Babić, Z. Dohćević-Mitrović, Z. V. Popović, Mater. Res. Bull. **48** (2013) 1363-1371

[40] J. Moreira, B. Serrano, A. Ortiz, H. de Lasa, Chem. Eng. Sci. **78** (2012) 186-203.

ALEKSANDAR GOLUBOVIĆ[1]
IVANA VELJKOVIĆ[2]
MAJA ŠĆEPANOVIĆ[1]
MIRJANA GRUJIĆ-BROJČIN[1]
NATAŠA TOMIĆ[1]
DUŠAN MIJIN[3]
BILJANA BABIĆ[4]

[1]Institut za fiziku, Univerzitet u Beogradu, Pregrevica 118, 11080 Beograd, Srbija
[2]Institut za multidisciplinarna istraživanja, Univerzite u Beogradu, Kneza Višeslava 1, 11000 Beograd, Srbija
[3]Tehnološko-metalurški fakultet, Univerzitet u Beogradu, Karnegijeva 4, 11000 Beograd, Srbija
[4]Institut za nuklearne nauke „Vinča", Univerzitet u Beogradu, 11001 Beograd, Srbija

NAUČNI RAD

# UTICAJ NEKIH PARAMETARA SOL-GEL SINTEZE MEZOPOROZNOG $TIO_2$ NA FOTOKATALITIČKU DEGRADACIJU ZAGAĐIVAČA

*Nanoprahovi titan-dioksida ($TiO_2$) su proizvedeni sol-gel tehnikom iz tetrabutil-titanata kao prekursora, varirajući neke parametre sol-gel sinteze kao što su temperatura kalcinacije (500 i 550 °C) i dužina kalcinacije (1,5; 2 i 2,5 h). XRPD rezultati su pokazali da su svi sintetizovani nanoprahovi dominantno u anataz fazi sa prisustvom malih količina rutilne faze u uzorcima kalcinisanim na 550 °C. Saglasno rezultatima dobijenim Williamson-Hall metodom, kristaliti anataza rastu sa vremenom kalcinacije (od 24 do 29 nm u uzorcima kalcinisanim na nižoj temperaturi, i od 30 do 35 nm u uzorcima kalcinisanim na višoj temperaturi). Analize pomeraja i poluširine najintenzivnijeg Eg Ramanskog moda anataza su potvrdile XRPD rezultate. Parametri veličine pora dobijeni pomoću eksperimentalnih podataka sorpcije azota su ukazali na to da su svi uzorci mezoporozni, sa srednjom veličinom pora u opsegu 5-8 nm. Fotokatalitička aktivnost dobijenih nanoprahova je testirana na degradaciji tekstilne boje (C.I. Reactive Orange 16), karbofurana i fenola.*

*Ključne reči: nanostrukture, anataz, difrakcija X-zraka na prahu, rasipanje.*